Three-Dimensional Structure Determination of a Protein Supercomplex That Oxidizes Methane to Formaldehyde in *Methylococcus capsulatus* (Bath)†

Natalia Myronova,‡,§ Ashraf Kitmitto,*,‡,∥ Richard F. Collins,⊥ Aki Miyaji,§ and Howard Dalton*,§

Department of Biological Sciences, University of Warwick, Coventry CV4 8EZ, U.K., Cardiovascular and Endocrine Division, School of Medicine, University of Manchester, Manchester M13 9NT, U.K., and Faculty of Life Sciences, University of Manchester, Manchester M60 1QD, U.K.

Received June 28, 2006; Revised Manuscript Received August 3, 2006

ABSTRACT: The oxidation of methane to methanol in methanotrophs is catalyzed by the enzyme methane monooxygenase (MMO). Two distinct forms of this enzyme exist, a soluble cytoplasmic MMO (sMMO) and a membrane-bound particulate form (pMMO). The active protein complex termed pMMO−C was purified recently from *Methylococcus capsulatus* (Bath) (*1*). The complex consists of pMMO hydroxylase and an additional component pMMO−R, which was proposed to be the reductase for the pMMO complex. Further study of this complex has led here to the proposal that the pMMO−R is in fact methanol dehydrogenase, the subsequent enzyme in the methane oxidation pathway by methanotrophs. We describe here the biochemical and biophysical characterization of a stable purified complex of pMMO hydroxylase (pMMO−H) with methanol dehydrogenase (MDH) and report the first three-dimensional (3D) structure, determined by cryoelectron microscopy and single particle analysis to ∼16 Å resolution. The 3D structure reported here provides the first insights into the supramolecular organization of pMMO with MDH. These studies of pMMO−MDH complexes have provided further understanding of the structural basis for the particular functions of the enzymes in this system which might also be of relevance to the complete process of methane oxidation by methanotrophs under high copper concentration in the environment.

Methanotrophic bacteria use methane as their sole carbon and energy source and therefore are of significant interest in terms of playing a key role in the cycling of carbon in the biosphere (*2*). There is also a significant potential for the commercial use of methanotrophic bacteria for the biotransformation of numerous organic chemicals into valuable products and the production of useful metabolites (*3*) as well as for the bioremediation of toxic pollutants (*4*, *5*). The methane oxidation pathway in the *Methylococcus capsulatus* (Bath) is shown in Scheme 1.

Scheme 1

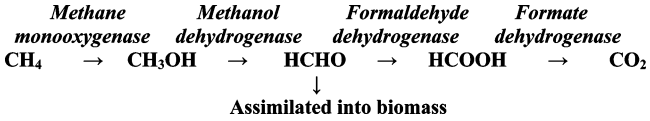

The first enzyme in this pathway, methane monooxygenase (MMO),[1] exhibits the unique catalytic capacity for converting methane to methanol under ambient conditions using dioxygen as the oxidant. Methane monooxygenases exist in two distinct forms: a soluble (sMMO) and a membrane-associated (pMMO) form. The regulation of expression of MMOs is governed by the level of copper in the environment (*6*−*8*). Both enzymes are multicomponent, comprising a metal-containing hydroxylase and electron-donating reductase. In addition, sMMO is associated with a regulatory protein (*9*). There is a low sequence homology between sMMO and pMMO (*10*, *11*) and little similarity with respect to their structural organization (*12*, *13*), substrate profiles (*14*), their need for metal cofactors (*1*, *15*−*17*), electron donors (*18*, *19*), or location within the cell (*6*). While sMMO is a well-characterized protein, pMMO has, until recently, remained elusive in terms of structure, location, and mechanism of action of the active site. The natural electron donor(s) and electron-transfer pathway in vivo have not been identified completely, despite intensive study. Even less is known about the spatial organization of the methane pathway in methanotrophs in the copper-rich environment when the intracytoplasmic membranes (ICMs) are developed extensively within the cell.

There is evidence that methanol dehydrogenase (MDH), a well-characterized periplasmic protein (*20*), may also be colocalized within the ICM network in the organism when expressing pMMO (*21*−*23*). Recently, a protocol was developed for the purification of an active protein complex termed pMMO−C from *M. capsulatus* (Bath) (*1*). The

† This research was supported by Grant 88/B13749 from the BBSRC to H.D. A.K. holds a British Heart Foundation Basic Science Lectureship Award.

* Corresponding authors. A.K.: e-mail, ashraf.kitmitto@manchester.ac.uk; tel, +44 (0)1613064186; fax, +44 (0)161 2751183. H.D.: e-mail, H.Dalton@warwick.ac.uk; tel, +44 (0)247 6523552.

‡ Both of these authors contributed equally to this study.

§ University of Warwick.

∥ Cardiovascular and Endocrine Division, School of Medicine, University of Manchester.

⊥ Faculty of Life Sciences, University of Manchester.

[1] Abbreviations: MMO, methane monooxygenase; pMMO, particulate methane monooxygenase; MDH, methanol dehydrogenase; ICM, intracytoplasmic membrane; DDM, dodecyl β-D-maltoside; PIPES, 1,4-piperazinebis(ethanesulfonic acid, sodium salt); BN-PAGE, blue native polyacrylamide gel electrophoresis; SDS−PAGE, sodium dodecyl sulfate−polyacrylamide gel electrophoresis; DTSSP, dithiobis(sulfosuccinimidyl propionate); SPA, single particle analysis.

10.1021/bi061294p CCC: $33.50
Published on Web 08/31/2006

complex pMMO−C was shown to consist of pMMO hydroxylase (pMMO−H), which was comprised of three subunits (Pmo A, Pmo B, Pmo C) and an additional component formed by two polypeptides with molecular masses of 63 and 8 kDa. It was suggested by these authors that this component was a potential candidate for the reductase of the pMMO complex and accordingly was designated as pMMO−R. Further extension of this work has now led here to the proposal that pMMO−R is in fact methanol dehydrogenase (MDH). We present here a biochemical characterization of a purified pMMO−C and show that it is comprised of both pMMO−H and MDH. Furthermore, we report the first three-dimensional (3D) structure of pMMO−C using single particle analysis (SPA) of the purified complex using cryonegative staining techniques.

EXPERIMENTAL PROCEDURES

Cultivation of M. capsulatus (Bath). All experiments described here use the *M. capsulatus* (Bath) from the University of Warwick culture collection. Methanotrophs were grown in nitrate minimal salt medium (*24*) with a final $CuSO_4$ concentration of 40 μM. Large-scale fermentation of *M. capsulatus* (Bath) was performed in a 100 L fermenter as described earlier (*1*). Cells were harvested and washed with 25 mM PIPES, pH 7.2, and resuspended in the same buffer. Concentrated cells were frozen and stored at −80 °C.

Membrane Isolation, Solubilization, and Purification of pMMO−C. Membrane isolation and subsequent solubilization was performed as described in refs *1* and *25*. The purification of the pMMO complex was carried by gel filtration on a Superdex 200 preparative-grade XK 16/200 column. Concentrated solubilized pMMO was applied to the precooled (4 °C) S200 column which was equilibrated with 25 mM PIPES, pH 7.2, supplemented with 0.03% (w/v) dodecyl β-D-maltoside and 1 mM benzamidine. The eluted fractions were checked for composition by SDS−PAGE (*1*). The fractions contained only pMMO−H and the 63 kDa proteins, referred to as pMMO−C, and were concentrated using an Amicon stirred cell with a XM-50 ultrafiltration membrane. Samples were stored at −80 °C after flash-freezing in liquid nitrogen.

Purification of MDH. Methanol dehydrogenase (MDH) was purified from the soluble fraction following cell disruption. The soluble fraction was loaded on DEAE-Sepharose F.F. (HR 26/10) column equilibrated with 20 mM Tris-HCl, pH 8.0. The fractions were collected, followed by concentration using an XM50 membrane (Millipore). The concentrated fraction was loaded onto a Superdex 200 (HR16/200) column equilibrated with 20 mM MOPS, pH 7.0, containing 0.1 M NaCl. Those fractions showing MDH activity and absorbance at 340 nm (from PQQ in MDH), but not 420 nm (from contaminating cytochrome), were collected and pooled. The pooled fraction was concentrated using ultrafiltration and checked for purity by SDS−PAGE.

Protein Concentration. Protein concentration was determined according to a modified Lowry protocol (*26*) with bovine serum albumin as standard.

Enzyme Activity Assay. (A) pMMO Activity. The activity of pMMO at each stage of membrane isolation and purification was assayed by following oxidation of propylene to propylene oxide by gas chromatography as described previously using duroquinol as electron donor (*25*).

(B) MDH Activity. Dye-linked oxidation of methanol was measured at 600 nm (*27*). The enzyme sample was incubated in 50 mM Tris-HCl (pH 9.0) containing methanol (10 mM), NH_4Cl (15 mM), KCN (5 mM), and dichlorophenolindophenol (DCPIP, 0.1 mM); the reaction was initiated by adding the mediator phenazine ethosulfate to 10 mM and the activity estimated from the decrease in absorbance at 600 nm due to reduction of DCPIP, using an absorption coefficient of 1.91×10^4 M^{-1} cm^{-1}.

Gel Electrophoresis. Blue native polyacrylamide gel electrophoresis (BN-PAGE) was carried out with a 5−13% polyacrylamide gradient gel, prepared by the method of Schägger and von Jagow (*28*, *29*). Samples (50−100 μg of protein per lane) were mixed with 0.5 M aminocaproic acid and loaded on the top of a 4% stacking gel. The gel was run at 8 °C at 16 mA constant current and 70−120 V. When the samples had completely passed through the stacking gel, the voltage was gradually increased to 300 V. The 0.02% Coomassie-containing cathode buffer was used until the dye front was one-third of the way from the top of the gel when it was replaced with 0.002% Coomassie-containing buffer. Following electrophoresis, gels were further destained in 25% methanol and 10% acetic acid. To determine the molecular mass of pMMO−C, several standard proteins with known molecular masses were used: thyroglobulin, 669 kDa; ferritin, 440 kDa; catalase, 232 kDa; lactate dehydrogenase, 140 kDa; albumin (bovine serum), 66 kDa. SDS−PAGE (12%) was performed according to Laemmli (*30*) at room temperature at 200 V. Protein bands on the SDS−PAGE gels were visualized by Coomassie brilliant blue R-250 (0.1% w/v) in 10% (v/v) methanol and 10% (v/v) glacial acetic acid. The gel was then destained by incubation in a solution of methanol−glacial acetic acid−water (4:1:5 v/v). The SDS−PAGE gels were calibrated using Dalton Mark VII-L markers (Sigma).

Chemical Cross-Linking Experiments. Cross-linking of the water-imposed domain of pMMO in the membrane fractions and pMMO−C was performed using dithiobis(sulfosuccinimidyl propionate) (DTSSP), a membrane-impermeable cross-linker, which cross-links only those proteins at the surface of the membrane fractions. The pMMO−C was diluted to 1 mg of protein/mL in 20 mM MOPS buffer, pH 7.2. DTSSP (20 mM), dissolved in 20 mM MOPS buffer, pH 7.2, was prepared immediately before use and added to the pMMO−C at a range of concentrations, 1−10 mM. The cross-linked samples were incubated on ice for 2 h. The reactions were quenched by the addition of Tris-HCl buffer, pH 7.5, to a final concentration of 50 mM and incubated for 15 min at room temperature. After quenching, the cross-linked samples were separated by BN-PAGE.

Analytical Gel Filtration. Calibration of Superdex 200 (Amersham Pharmacia Biotech) (HR10/300) for molecular mass estimation was carried out by equilibrating the column with 25 mM PIPES, pH 7.2, containing 0.03% (w/v) *n*-dodecyl β-D-maltoside at a flow rate of 0.3 mL/min. The molecular mass determination of pMMO−C was made by comparing the ratio V_e/V_o of pMMO−C with the ratio V_e/V_o of four proteins of known molecular mass (Bio-Rad calibration kit: aldolase, 158 kDa; catalase, 232 kDa; ferritin, 440 kDa; thyroglobulin, 669 kDa), where V_e is the elution volume and V_o is the void volume of the column, which was taken as the elution volume required for the elution of Blue Dextran

(2000 kDa) from the column. The calibration curve was prepared by plotting the logarithms of the known molecular masses of protein standards against their V_e/V_o values. The corresponding molecular masses could then be deduced from the calibration curve by using the experimentally determined V_e/V_o value of pMMO−C.

Analytical Ultracentrifugation. Sedimentation Velocity and Sedimentation Equilibrium Analysis. Analytical ultracentrifugation experiments were conducted in the National Centre for Molecular Hydrodynamics (NCMH) Business Centre at the University of Nottingham, U.K.

(A) Sedimentation Velocity. The experiments were performed at 20 °C in 25 mM PIPES, pH 7.2, in a Beckman XL-A analytical ultracentrifuge (Palo Alto, CA), following the Standard Operating Procedure SV01_02. Optical path length centerpieces of 12 mm were used in the cells. An initial scan was performed at 3000 rpm to check for the presence of heavy aggregates. A final rotor speed of 35000 rpm was selected, and 100 scans at 375 nm were taken at 6 min intervals and logged to disk using the Beckman software. The program SEDFIT was used for data analysis, following the protocol prescribed in Standard Operating Procedure SVA-02 (*31*, *32*).

(B) Sedimentation Equilibrium. The experiments were performed at 20 °C in a Beckman XL-I analytical ultracentrifuge, following the Standard Operating Procedure SE-IO_04.1 using interference optics. Optical path length centerpieces of 12 mm were used in the cells. After recording initial scans at 3000 rpm, a final rotor speed of 7000 rpm was selected. Scans were taken every 60 min and data logged to disk using the Beckman software. Final scans were accepted for analysis when no significant detectable changes could be found between successive scans.

The calculation of the molecular masses of the samples was carried out using newly written local software, the Mfit suite (manuscript in preparation from Prof. Arthur Rowe, University of Nottingham). The function Mfit is obtained by simple integration with respect to r^2 (r = radial position) of the basic equation for sedimentation equilibrium and is defined by

$$\int y_i \, d(r^2) = \int_{r-a}^{r-b} f(r^2) = (2c_a/\sigma_w) \exp[0.5\sigma_w(r^2 - r_a{}^b) - 1] + E(r^2 - r_a{}^b)$$

where y_i are the data points, and their integration is performed numerically. The baseline offset is given by E, c is the solute concentration at a given radius, and c_a and r_a are the initial concentration and initial radial position, respectively. An estimate for the (reduced, flotational) molecular weight σ is obtained by nonlinear fitting, using the Levenberg−Marquadt algorithm.

Mass Spectrometric Analysis of the pMMO Complex. (A) Protein Identification by Means of On-Line Liquid Chromatography and Electrospray Ionization Mass Spectrometry (LC−ESI-MS/MS). Protein bands from BN-PAGE gels were excised, destained, reduced, alkylated, and digested with trypsin and the resulting peptides extracted using the Micromass Mass Prep Station running the standard digestion protocol supplied by the manufacturer. The extracted tryptic peptides were transferred to a Micromass modular CapLC and autosampler system. A 5 μL aliquot of extract was mixed with 15 μL of 0.1% formic acid and loaded onto a 0.5 cm LC Packings C18 5 μm 100 Å 300 μm i.d. μ-precolumn cartridge. Flushing the column with solution A desalted the bound peptides before a linear gradient of solution B at a flow rate of 0.2 nL min^{-1} eluted the peptides for further resolution on a 15 cm LC Packings C18 5 μm 5 Å 75 μm i.d. PepMap analytical column. The eluted peptides were analyzed on a Micromass QTof (or Ultima Global) mass spectrometer operated in positive ion mode, controlled by MassLynx 4.0 software and fitted with a nano-LC sprayer with an applied capillary voltage of 3.5 kV. The instrument was calibrated against a collisionally induced decomposition (CID) spectrum of the doubly charged precursor ion of Glu-fibrinopeptide B. The instrument was operated in data-dependent acquisition (DDA) mode over the mass/charge (m/z) range of 50−2000. During the DDA analysis, both MS and tandem mass spectrometries (CID) were performed on the most intense peptides as they eluted from the column. The MS/MS data were processed and searched against an appropriate database using the Micromass Global Server 2.0 search engine. Search parameters specify up to one missed cleavage site, a 0.25 Da tolerance against the database-generated theoretical peptide and product ion masses, and a minimum of 1 matched peptide. A list of the 20 highest scoring entries was produced, and each suggested protein identification was confirmed or rejected by a comparison of the theoretical sequence with observed MS/MS data. When the database searches were unsuccessful, the MS/MS spectra were interpreted in order to obtain amino acid sequence tags. Spectra were interpreted either manually or automatically using the Micromass MassSeq software package or by a combination of the two probabilistic sequences suggested.

(B) Protein Identification by Means of MALDI. The intact molecular mass of the small subunit of MDH from *M. capsulatus* (Bath) was determined by means of matrix-assisted laser desorption ionization (MALDI) mass spectrometry using a TofSpec 2E (Micromass, Manchester, U.K.) instrument which was operated in linear mode at an accelerating voltage of 20 kV. A VSL-337i nitrogen laser (Laser Science Inc., Newton, MA) was employed, operating at 337 nm, under control of the MassLynx (Micromass, Manchester, U.K.) data system. The sample was added to the matrix solution (10 mg/mL sinapinic acid in 50:50 acetonitrile−0.1% trifluoroacetic acid in H_2O) to a final concentration of 1 μM, and a 1 μL aliquot was spotted onto the target and allowed to dry, prior to analysis. Calibration was achieved using a sample prepared in an identical manner, containing the proteins cytochrome *c* and myoglobin over the m/z range 5000−20000. Approximately 200 laser shots were employed to obtain the mass spectrum. The combined spectrum was smoothed and background subtracted to derive an average molecular mass for the protein species.

Electron Microscopy. pMMO−C was resuspended in 25 mM Pipes buffer (pH 7.25) containing 100 mM NaCl and 0.01% (w/v) *n*-dodecyl β-D-maltoside for a concentration of ~100 μg/mL. Samples were initially examined using standard negative staining techniques with 2% (w/v) uranyl acetate as described in refs *25* and *33*. For the 3D structure determination a 20 μL aliquot of pMMO−C was mixed with an equal volume of 10% (w/v) ammonium molybdate (pH 7) and 2% (w/v) trehalose. Carbon-coated, glow-discharged grids were then incubated on a 20 μL droplet of the purified

Table 1: Methane Monooxygenase and Methanol Dehydrogenase Activity of pMMO-Containing Samples

sample	pMMO activity [nmol of propylene oxide produced min^{-1} (mg of protein)$^{-1}$] with 10 mM duroquinol as reductant	MDH activity [μmol of O_2 min^{-1} (mg of protein)$^{-1}$]
pMMO−C	69 ± 9	0.25 ± 0.2
pMMO−H	25 ± 6	no activity

pMMO−C embedded in ammonium molybdate−trehalose for 30 s and blotted (Whatman 50 filter paper) and examined in a Philips 200 (FEG) TEM equipped with an Oxford system cryostage under low temperatures (~100 K) and low dose conditions (<15 electrons/Å^2). Images were collected using a 4K × 4K CCD camera at a magnification of 48234× for 3.1 Å/pixel at the specimen level and between −1.7 and 2.5 μm defocus range.

3D Image Processing of pMMO−C. The 3D structures of pMMO−C were generated using the common line projection matching methods employed in EMAN (*34*). The contrast transfer function (CTF) was determined for each image using CTFIT (part of the EMAN software). Approximately 7500 pMMO−C complexes were selected interactively using the graphical interface boxer (EMAN processing software) into a box of 72 × 72 pixels (223 × 223 Å). A preliminary 3D model was calculated from a set of reference-free class averages that represented distinct views of the complex, generated after band-pass filtering and centering of the particles. The preliminary 3D model was iteratively refined using a projection matching routine, whereby projections with uniformly distributed orientations of the preliminary 3D model were used as references for classification of the raw data set, with the class averages from this step used to construct a new 3D model. Convergence, i.e., stabilization of the 3D structure, was monitored by examining the Fourier shell correlation (FSC) of the 3D models generated from each iteration. Volumes were separately calculated with either C1, C2, C3, or C4 symmetries applied. For the C1 and C2 volumes the class averages used to generate the preliminary model were selected by the user. In each reconstruction the final 3D volume was derived from eight rounds of iterative refinement. The resolution of each reconstruction was assessed following established procedures (*35*, *36*). In brief, the data set was divided into two, with volumes calculated for the two subsets, and the resolution was estimated by the Fourier shell correlation coefficient (FSC) with the resolution limit taken to be where the FSC value fell below 0.5.

RESULTS

Purification of pMMO−C. The specific activities of the purified pMMO complex (pMMO−C) and pMMO hydroxylase (pMMO−H) are presented in Table 1 illustrating that the activity of pMMO−C is approximately twice that of pMMO−H alone, using duroquinol as reductant. Analysis of the polypeptide composition of pMMO−C by SDS−PAGE (Figure 1) indicates that the principal polypeptides have molecular masses at 63, 45, 26, and 23 kDa and a weaker band at ~32 kDa. The additional protein with a molecular mass at 8195.9 Da was observed in the pMMO−C samples by means of MALDI. The 45, 26, and 23 kDa bands have been previously reported as components of pMMO−H

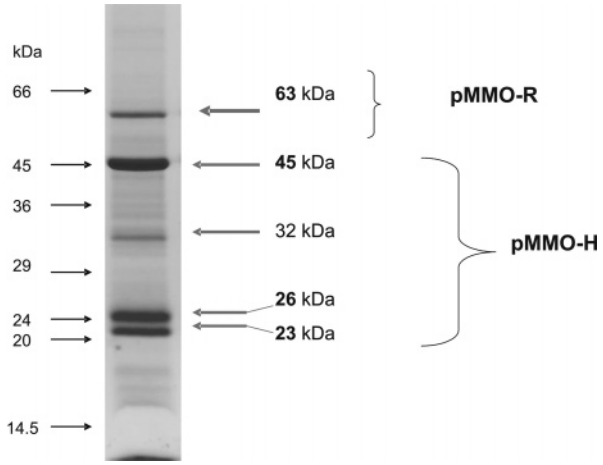

FIGURE 1: 12% SDS−PAGE of the purified pMMO complex (pMMO−C) from *M. capsulatus* (Bath) stained with Coomassie brilliant blue R-250.

(*37*) corresponding to polypeptides β (PmoB subunit), α (PmoA subunit), and γ (PmoC subunit). A weaker band at ~32 kDa was also observed in purified samples of pMMO−H and was suggested to be a proteolytic product of the β subunit (*15*). The additional polypeptides found to comprise purified pMMO−C, namely, the 63 and 8 kDa bands, have previously been designated as pMMO−R, the possible reductase component in the complex (*1*).

Identification of Putative pMMO Reductase (pMMO−R) as Methanol Dehydrogenase (MDH). The 63 kDa protein band in Figure 1 was excised and incubated with trypsin, and the digest was analyzed by MALDI-MS. Peptide fingerprinting revealed 32% coverage with 75% identity for the large subunit of methanol dehydrogenase (mxaF) based on the sequence from *M. capsulatus* (Bath) (*10*). The molecular mass of the smallest subunit of pMMO−C was estimated as 8195.9 Da by means of MALDI . These data indicate that pMMO−R (~63 and 8.2 kDa) is likely to be methanol dehydrogenase (~66 and 8.5 kDa) ((*20*) and is referred to in this report from now on as MDH. This conclusion was further supported by experiments revealing that pMMO−C, but not the pMMO hydroxylase alone, could oxidize methanol to formaldehyde in the presence of the 2,6-dichlorophenolindophenol (DCPIP) as the terminal electron acceptor with a specific activity of 0.25 μmol of O_2 min^{-1} (mg of protein)$^{-1}$ (Table 1). Since, MDH is an important component of the pMMO complex, it can be inferred that methanol dehydrogenase interacts with the pMMO hydroxylase to form an efficiently functioning pMMO complex in vitro.

Molecular Mass Estimation of the pMMO Complex. Several methods were employed to investigate the molecular mass of the pMMO complex. Using analytical gel filtration, the value, in the presence of bound detergent, was estimated as 438.4 kDa (Figure 2). BN-PAGE revealed a single protein band (Figure 3A, lane 2) with a molecular mass of ~440 kDa, suggesting that pMMO−C exists as a stoichiometric complex. The migration of the pMMO−C is retarded when compared with MDH (lane 4) and pMMO−H (lane 3), indicating a larger mass for the complex. In addition, no individual subunits, other subcomplexes, or larger oligomers were detected on the gel. The molecular mass of the purified MDH (Figure 3A, lane 4), which also ran as a single band, was estimated as 200−210 kDa. In duplicate experi-

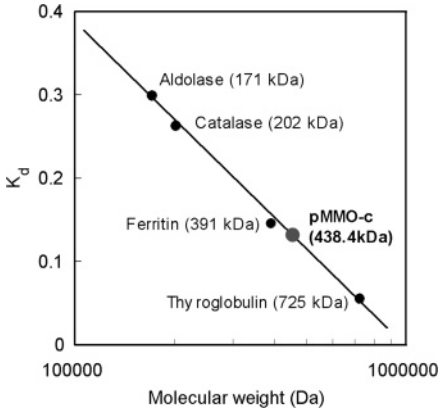

FIGURE 2: Molecular mass estimation of pMMO−C by analytical gel filtration. Gel filtration chromatography was undertaken using a Superdex 200 HR10/300 GL size-exclusion column. Molecular mass standards used to calibrate the column were aldolase (171 kDa), catalase (202 kDa), ferritin (391 kDa), and thyroglobulin (725 kDa). The approximate molecular mass of the detergent-bounded pMMO−C was estimated to be 438.4 kDa.

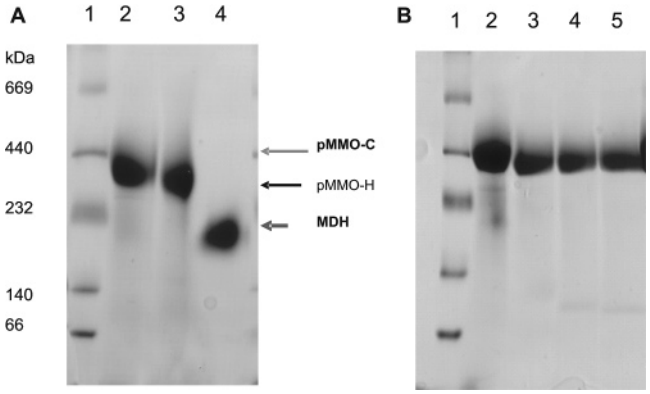

FIGURE 3: 5−13% Blue native PAGE of pMMO−C. (A) Lane 1, high molecular mass protein standard for native electrophoresis, thyroglobulin (669 kDa), ferritin (440 kDa), catalase (232 kDa), lactate dehydrogenase (140 kDa), and albumin (bovine serum) (66 kDa); lane 2, purified pMMO−C from a Superdex 200 column (60 μg); lane 3, pMMO−H (60 μg); lane 4, purified MDH from the Superdex 200 column (50 μg). (B) Lane 1, HMW protein standard for native electrophoresis, as in (A); lane 2, purified pMMO−C; lane 3, pMMO−C + 2 mM DTSSP; lane 4, pMMO−C + 5 mM DTSSP; lane 5, pMMO−C + 7 mM DTSSP.

ments the 440 kDa protein band (lane 2) was digested with trypsin and characterized by means of LC−ESI-MS/MS. The presence of pMMO−H was identified by sequence identity of all three subunits of pMMO−H. The presence of methanol dehydrogenase was also confirmed by sequence identity of two peptides from methanol dehydrogenase large subunit mxaF.

To eliminate the possibility that there were separate components within the complex, the purified pMMO−C sample was also treated with increasing concentrations of the cross-linker DTSSP, and the cross-linked product was analyzed by BN-PAGE (Figure 3B). A comparison of the untreated (Figure 3B, lane 2) protein and protein incubated with increasing amounts of DTSSP (lane 3−5) gave only a single high molecular mass polypeptide band at ~440 kDa.

The oligomeric state of the pMMO−C was also examined by sedimentation velocity data analysis. The sedimentation coefficient distribution *c*(*s*) profile of pMMO−C (Figure 4)

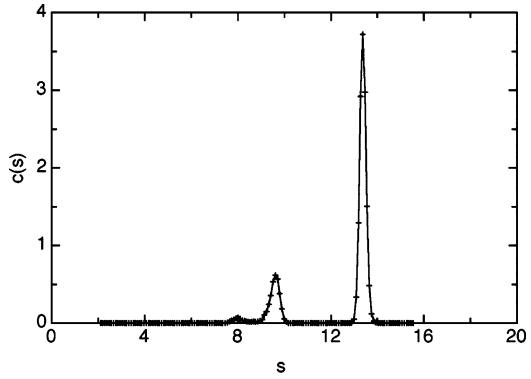

FIGURE 4: Sedimentation velocity analysis of pMMO−C. Sedimentation velocity experiments were performed at 20 °C in 25 mM PIPES, pH 7.2. The protein concentration was 9 mg/mL. A wavelength of 375 nm and a final rotor speed of 5300 rpm was employed.

shows the presence of a major peak around 13.5 S, with the minor peaks (estimated: 18% of total) around 10 and 8 S. From this we presume that about 82% of the protein exists in the native state. The presence of the minor components could be caused by partial denaturation of protein complex under experimental conditions, which included running the centrifuge at 20 °C. Knowing that the majority of the pMMO−C complex is in the monodisperse state, its molecular mass was estimated using sedimentation equilibrium analysis. Assuming a value of 0.81 mL/mg for the partial specific volume of the protein complex plus detergent, the molecular mass for pMMO−C was calculated as 687 kDa.

3D Structure of a pMMO−MDH Complex (pMMO−C). Samples of the purified pMMO−C were initially examined using negative staining techniques to assess the homogeneity of the sample. A field of pMMO−C complexes are shown in Figure 5A, revealing a homogeneous sample of well-dispersed, uniformly sized, particles with only a few small areas of aggregation observed. For the 3D structure determination of the complex we employed cryoelectron microscopy of purified pMMO−C embedded in trehalose−molybdate (see Experimental Procedures). The inset to panel A shows an example of a fast Fourier transform (FFT) of one of the micrographs collected under cryo-EM conditions. Panel B of Figure 5 shows class averages of the cryoimages after CTF correction using reference-free two-dimensional projection classification. These images have been low-passed filtered (18 Å) for clarity. Examination of these class averages (no symmetry applied) finds distinct views of pMMO−C. Particles 1 and 2 show rounded complexes ~100 Å in diameter with a central cavity, whereas particles 3−6 are larger with dimensions of approximately 150 × 100 Å. The class averages in groups 7 and 8 show particles similar in size and overall shape to those in groups 1 and 2 but without the central indentation.

We calculated the 3D structure of the purified pMMO−C with C1, C2, C3, and C4 symmetries, with the top and side views for each volume shown in Figure 5C. Examination of the C2 refined structure finds the side view is only ~ 90 Å in height and therefore is smaller than that reported for purified pMMO−H determined by both electron microscopy (*25*) and X-ray crystallography methods (*13*). Both the C1, C3, and C4 structures have side views approximately 140 Å tall, composed of two separate domains. Also common to

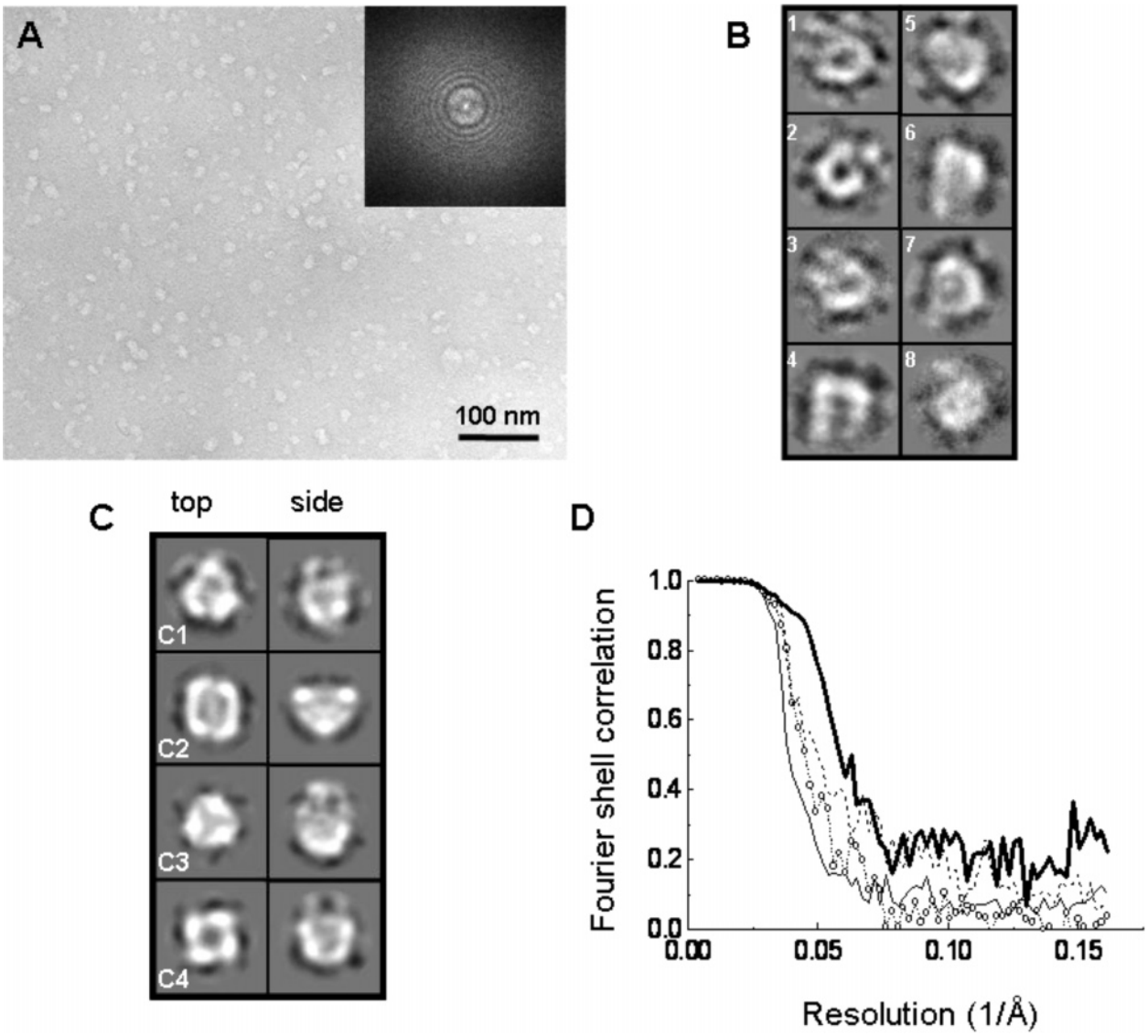

FIGURE 5: TEM and image processing data of purified pMMO−C. (A) A field of negatively stained (2% w/v uranyl acetate) purified pMMO−C, illustrating that the particles are uniformly dispersed and homogeneous. Inset: Example of a fast Fourier transform of a micrograph used for the 3D reconstruction of purified pMMO−C examined under cryo-EM conditions after embedding in trehalose−molybdate. The edge of the transform corresponds to 1/6.2 Å. (B) A selection of 2D class averages calculated from the cryonegative particle raw data set using reference-free alignment in EMAN (*34*). (C) Preliminary 3D models of pMMO−C determined by applying C1, C2, C3, and C4 symmetries. The left column shows the top view and the right column the side view of each reconstruction. (D) Fourier shell correlation (FSC) resolution estimate for each of the 3D volumes of pMMO−C with C1, C2, C3, and C4 symmetry applied (solid line, circle symbols, dashed line, and solid black line, respectively) illustrating that at FSC = 0.5 the C3 model has the highest resolution of ∼16 Å.

both the C1 and C3 structure is the triangular-shaped top view comprised of three protein densities that is distinct from the more square-shaped C2 and four-lobed C4 top views. Panel D of the figure shows the plot of the Fourier shell correlation (FSC) against resolution for each of the four models: 25 Å (C1), 22 Å (C2), 19 Å (C4) finding the C3 structure having the highest resolution of ∼16 Å. C3 symmetry was selected as most appropriate for determining the 3D structure of pMMO−C based on the biochemical and image analysis data reported here and coupled with previous data from this group (*25*) and others (*13*) that demonstrated that purified pMMO−H is trimeric.

The 3D structure of pMMO−C is displayed in Figure 6 at a threshold that encompasses a mass of ∼530 kDa. The intracellular side of the complex is shown in panel A presenting a triangular-shaped density ∼110 Å across (edge to edge). Rotation of this view of pMMO−C by 180° reveals that the putative periplasmic view is also triangular in shape, characterized by three protein densities, forming a three-pronged star. Presented in panel C (rotation of the complex in B around the *x*-axis by 90°) is the side view of pMMO−C, i.e., perpendicular to the membrane plane, which is approximately 160 Å tall and is comprised of two distinct domains: a cylindrically shaped region we have termed the "body" (∼105 Å tall) associated with a domain we have termed the "cap" which is composed of three protein segments, each of which interacts with the body. The regions of the body that forms the contacts with the cap are distinct densities we have termed "arms", features we also reported in the pMMO−H structure determined by EM and SPA methods (*25*). One of the arm domains enclosed by the dashed box has been enlarged (inset) and displayed at 2.5σ above the mean density to reveal that each arm is punctuated by a small hole that runs through to the interior, a structural

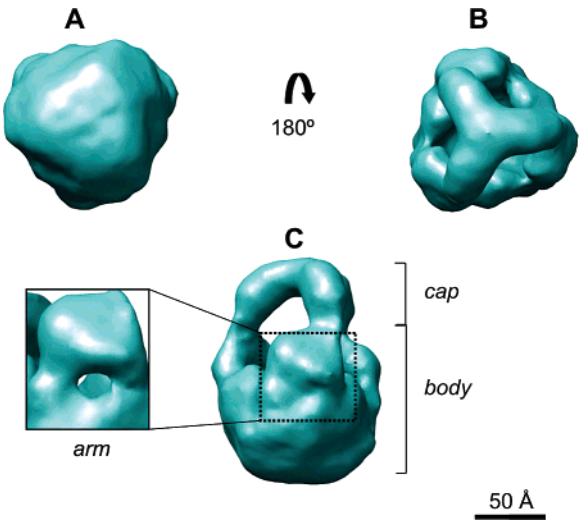

FIGURE 6: 3D structure of pMMO−C. The 3D volume of pMMO−C refined with C3 symmetry applied displayed at thresholds (1.8σ above the mean density) to encompass a complex with a mass of ~530 kDa. (A) Putative intracellular side of pMMO−C showing a relatively flat complex triangular in shape. (B) Putative periplasmic face of pMMO−C revealing three protein densities joining in the center to form a three-pronged star arrangement. (C) Putative side view of pMMO−C illustrating that the purified complex is composed of two densities termed the cap and body. The expanded area shows that the upper portion of the body we called the arm. Densities are characterized by a region of low density (displayed at 2.5σ above the mean density) that runs through from the external surface into the interior of the structure.

motif also reported for the EM pMMO−H volume (*25*) and matched with low-density regions in the crystal structure (*13*). Also in common with the pMMO−H structure is the central channel running through pMMO−C in the region termed the body. Figure 7 shows the interior of the complex by removing half of the structure (panel A). The cut-away in panel A shows that the central cavity is cone-shaped unlike the cylindrical channel, with a uniform diameter, of pMMO−H. At the mouth of the body domain there is a small central density, but it is not clear whether this is an artifact or a feature of the structure. The interior features of pMMO−C were also examined by taking slices through the height of the volume from the putative intracellular side through to the periplasmic side (Figure 7B). Slice 9 in panel B finds the cavity of pMMO−C is ~20 Å in diameter widening to ~65 Å in slice 26. Though the cap does not seal the cavity off from the extracellular milieu, it can be seen to partially occlude it (slices 27−32). The three protein densities composing the cap are clearly defined in sections 40 onward. What is also apparent from the slices is that in the region corresponding to the body (slices 1 to ~34) there is a twisting of the protein domains by ~35° in a clockwise direction. The EM volume of pMMO−H also revealed a similar skewing of the base and neck of the structure by ~60°. The view of pMMO−C in Figure 6A shows that the structure is sealed from the cytosolic side of the membrane; however, when displayed at higher thresholds a central cavity forms; therefore, coupled with the fact that the cavity narrows toward the intracellular side of the membrane, we suggest that the complex may be open to the cytosol and that due to the presence of a detergent plug or a limit of the resolution of the structure it appears closed.

DISCUSSION

A recent crystal structure of the purified pMMO−H (2.8 Å resolution) showed that it formed a trimer, comprising α, β, and γ polypeptides, and roughly resembled a cylinder (*13*). We also presented a report demonstrating that pMMO−H was trimeric using electron microscopy and single particle analysis (*25*). We also demonstrated that the oligomeric complex was functional, with data that also suggested that a trimeric pMMO−H may likely represent the in vivo form. We have now advanced these studies by finding that two enzymes of the methane oxidation pathway in the *M. capsulatus* (Bath), pMMO−H and methanol dehydrogenase (MDH), form a supramolecular complex that we have called pMMO−C. The formation of a supracomplex is now being realized as a common theme in biological systems (*38*−*41*).

It is generally accepted that methanol dehydrogenase (MDH), a pyrroloquinole quinone (PQQ) containing enzyme oxidizing methanol to formaldehyde, is a periplasmic soluble protein (*20*). An X-ray structure has been determined for MDH from *Methylobacterium extorquens* (*42*) and *Methylophilus* sp. (*43*). MDH crystallized as a dimer ($\alpha_2\beta_2$) showing that each α subunit (66 kDa) contained one molecule of PQQ and one Ca^{2+} ion. The β subunit (8.5 kDa) was seen to fold around the α subunit though its function is unknown. The suggestion that a domain of MDH could be associated with intracytoplasmic membrane in methanotrophs was published 30 years ago (*23*) with new evidence recently presented (*21*). In the absence of structural information defining the interaction of pMMO and MDH our previous prediction of the interaction between the neighboring enzymes relied on biochemical data (*1*). In the present study, the association of pMMO−H and MDH in the stable complex has now been confirmed by means of BN-PAGE and analytical ultracentrifugation, with the biochemical data illustrating here that pMMO−C exists in a complex of at least two proteins.

We have examined the oligomeric state of the purified pMMO−C by analysis of the molecular mass of the components, both in their individual state and in the complex. The molecular mass of the MDH, purified from the complex, was confirmed as 200 kDa using BN-PAGE electrophoresis (Figure 3A, lane 4). Since the molecular mass for the monomer of MDH based on SDS−PAGE (Figure 1) and MS analysis was ~71 kDa, we infer that it exists in the trimeric state within the complex. Furthermore, it has already been established that pMMO−H also exists as a trimer with a molecular mass of 300−310 kDa (*25*). Thus we propose that the complex forms by association of two trimeric proteins with an expected molecular mass of around 510−520 kDa. In this study a molecular mass of the purified pMMO−C complex was estimated as 438 and 440 kDa, using analytical gel filtration and BN-PAGE electrophoresis, respectively. The lower value of the complex may be due to the difference in the shape of the complex compared with individual components. Such conformational differences can affect the mobility of proteins through the column matrix (*44*) or polyacrylamide gels (*28*). In this paper we have shown that the transmembrane helices and extracellular arm domains of pMMO−H undergo significant conformational rearrangement upon binding MDH, and this could well explain the molecular mass difference observed.

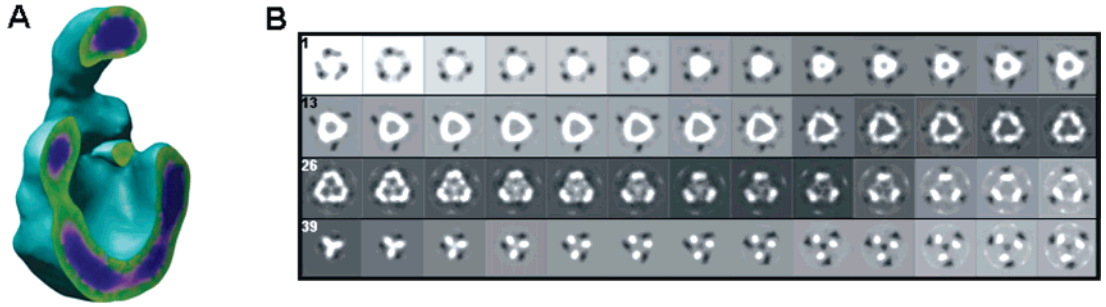

FIGURE 7: Slices through the pMMO−C 3D structure. (A) pMMO−C as viewed from the side (i.e., parallel to the membrane plane) with one-half of the structure removed to reveal the interior of the volume illustrating that the central cavity is narrower toward the putative intracellular side. At the plane of the cut-away the colors represent the protein density distribution (green = 2.7σ, pink = 2.8σ, navy blue = 3.6σ). (B) Sections (x−y plane) through pMMO−C as orientated in Figure 4A with slices at 3.1 Å intervals taken from the intracellular side. Box size = 223 × 223 Å.

Another explanation for the discrepancy between the expected and observed values for the total molecular mass of pMMO−C was that some components of the complex were lost during the analytical procedure. To test this, we treated the complex with the cross-linker DTSSP and determined the molecular mass of both untreated (Figure 3B, lane 2) and protein incubated with increasing amounts of DTSSP (lanes 3−5) by BN−PAGE. All samples gave only a single high molecular mass polypeptide band at ~440 kDa, demonstrating that pMMO−H and MDH are in close contact. The oligomeric state of the pMMO−C was also confirmed on the basis of the sedimentation velocity data analysis. The sedimentation coefficient distribution profile of pMMO−C (Figure 4) indicates that about 82% of the protein exists in the native state. At the same time, the molecular mass for pMMO−C, calculated from sedimentation equilibrium data, was 687 kDa including the bound detergent. Studies of other membrane-bound proteins have indicated that around 30−35% of the mass of the protein could be due to bound detergent (*45*). Assuming, therefore, that detergent has surrounded only the hydrophobic surface of the membrane protein, the resulting molecular mass of pMMO−C, measured by equilibrium sedimentation, should be as high as 540−560 kDa, in good agreement with the suggestion that both proteins in the complex exist as trimers.

Presented in Figure 8 is the 3D structure of pMMO−C matched with the crystal structures of both pMMO−H and MDH. Panel A shows that the height of the pMMO−C domain termed here as the body as viewed perpendicular to the membrane plane fits very closely with the side view of the pMMO−H crystal structure and has a similar width at the base. We propose that the body of pMMO−C is formed by pMMO−H and the cap domain is formed by a trimer of MDH. Rotation of this view in panel A by 90° around the x-axis away from the plane of the paper reveals the "top" view of the complex revealing that the domains of pMMO−H we have termed the arms, i.e., the extracellular portion, of the crystal structure do not overlay with the corresponding arm domains of pMMO−C. This is in contrast to our previous report describing the 3D structure of pMMO−H determined by EM/SPA methods of negatively stained samples (*25*) where the three densities designated as the arms were found to map onto the extracellular domains of the crystal structure. Panel C shows the 3D volume of pMMO−C with both the crystal and EM structures of pMMO−H. It was noted previously that the EM volume of

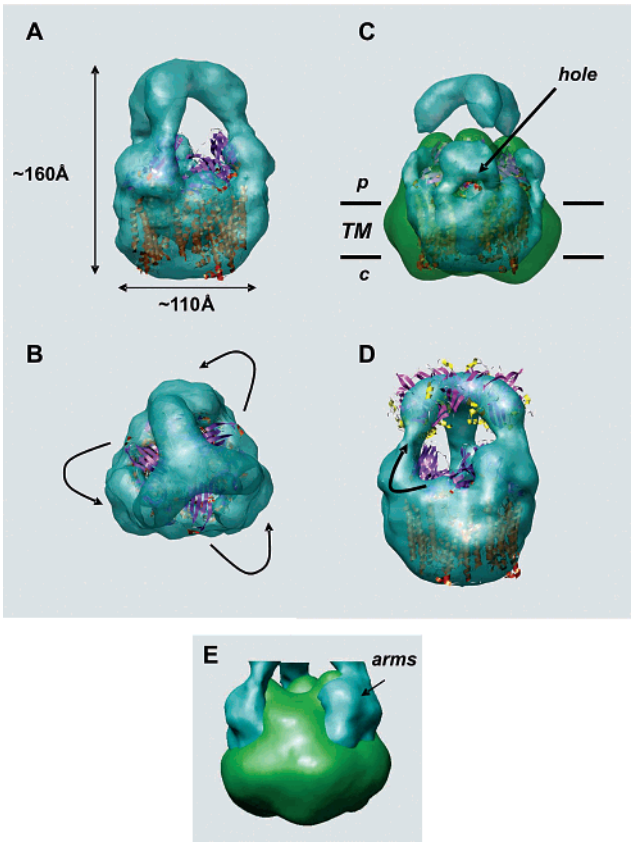

FIGURE 8: Comparison of the 3D structures of pMMO−C and pMMO−H. (A) Putative side view of pMMO−C with the X-ray structure of pMMO−H (PDB code 1YEW) fitted into the EM envelope illustrating that the body domain of pMMO−C matches with the height of pMMO−H. (B) Putative periplasmic view of the 3D volume of pMMO−C matched with the X-ray structure of pMMO−H. The curly black arrows indicate that the EM density of pMMO−C is rotated with respect to the extracellular portion of pMMO−H. (C) Putative side views of the EM volumes of pMMO−C (displayed at 2.5σ above the mean density) and pMMO−H (*25*) with the X-ray structure of pMMO−H fitted so that the regions of low density in the domain we have previously termed the arms are matched in all three structures. TM denotes the transmembrane region, p the periplasm, and c the cytosol. (D) 3D volume of pMMO−C with the crystal structure of an MDH dimer (PDB code 1G72) matched with two lobes of the cap domain. (E) 3D volume of pMMO−C with the cap domain removed to allow a comparison of the body domains of pMMO−C with the EM volume of pMMO−H previously determined by this group (*25*), illustrating a major conformational rearrangement of the arm densities of pMMO−C for interaction with the MDH trimer.

pMMO−H had an extra ring of density around the putative transmembrane domain that was not observed in the crystal structure and was ascribed as a ring of detergent micelles. It is interesting to note that, from the comparison of the three structures in panel C, it appears that the structure refinement of the purified pMMO−C, embedded in trehalose−molybdate and images collected under cryo-EM conditions, has not led to definition of the bulk detergent phase, and the dimensions in this region fit very well with the crystal structure. However, it is also apparent from panel C that the region of low density "holes" in the arm domains identified in both the EM and X-ray structure of pMMO−H is also a characteristic of the pMMO−C volume as shown in panel C. Panel E shows the EM volume of pMMO−H and pMMO−C with the cap removed, and this figure illustrates the major conformational changes that have occurred to the extracellular arm domains of pMMO−H on binding MDH leading to an outward tilting and twisting of the transmembrane domains. This agrees with the formation of a cone-shaped central channel (with a maximum diameter of 65 Å) in pMMO−C whereby the rearrangement of the body domain to interact with the MDH has led to a widening of the cavity compared to pMMO−H (∼20−25 Å diameter). Panel D shows the MDH crystal dimer structure (*20*) fitted into two of the lobes forming the trimeric cap. The geometry of the dimer can be seen to map well onto the electron density. It cannot be determined from this manual mapping of the crystal structure into the EM envelope which regions of MDH interact with pMMO−H but serves to demonstrate that the densities forming the cap correspond well to the dimensions of MDH.

The "screw-cap" mechanism for the assembly of the two enzymes, pMMO−H and MDH, leads to the formation of a "fitted structure". It has been emphasized repeatedly that the main problem in the study of the particulate methane monooxygenase is the production of active and stable purified enzyme (*15*, *46*, *47*). Usually, the specific activity of the pure pMMO−H is significantly less compared with membrane-embedded protein due to several reasons discussed recently (*25*). In this study we have shown that the specific activity of pMMO−H copurified with MDH was approximately 2-fold higher than the activity of purified pMMO−H alone. We suggest that the close association of the two enzymes has led to the structural stabilization of the labile pMMO−H. Another example of enzymes with lid and cap domains, which is important for the catalytic activity, is the gastric lipases. Removing these domains from the core protein leads to the loss of specific activity with the lipid substrate. These two elements, which appear structurally independent, cannot be separated to give a fully active enzyme which permits the correct fitting of the triglyceride molecule in the active site (*48*).

When *M. capsulatus* (Bath) was grown under high copper (pMMO-containing) conditions, the efficiency of conversion of methane into biomass was 38% higher than in cells grown under low copper (sMMO-containing) (*49*). Several explanations have been given for this increase in yield based largely on the provision of reductase for MMO. Soluble MMO is known to require NADH as the electron donor, and its supply in cells could well be the growth-limiting factor rather than ATP (*50*). The precise electron donor for pMMO, however, is unknown, but early observations in Higgins' group (*51*) suggested that electrons from the oxidation of methanol were recycled into the oxidation of methane. Such direct coupling could obviate the need for NADH (which is normally growth limiting) and thus resulted in high growth yield (*52*). It is interesting to note that the structure of pMMO−H also reveals a possible docking site for the reductase, a negatively charged patch on the outer surface of the soluble domains of the β subunit (*13*). It is tempting therefore to speculate that this is where MDH is bound to pMMO.

In summary, we can conclude that the assembly of two enzymes, pMMO and MDH, into a complex contributes to their stability and facilitates direct coupling of electron transport between them, leading to a more efficient utilization of methane into biomass.

ACKNOWLEDGMENT

The authors acknowledge the contributions of the Biological Mass Spectrometry and Proteomics Facility in the Department of Biological Sciences, University of Warwick, and Anthony Jackson at ICI Measurement Science Group, Wilton, Middlesbrough, U.K. We thank Prof. Arthur Rowe at NCMH, University of Nottingham. for the carrying out the analytical ultracentrifugation experiments and for useful discussion. The authors also thank Prof. P. Bullough and Dr. P. Wang, Sheffield University, for cryo-TEM advice and technical support.

REFERENCES

1. Basu, P., Katterle, B., Andersson, K. K., and Dalton, H. (2003) The membrane-associated form of methane mono-oxygenase from *Methylococcus capsulatus* (Bath) is a copper/iron protein, *Biochem. J. 369*, 417−427.
2. Smith, K., Dobbie, K., Ball, B., Bakken, L., Sitaula, B., and Hansen, S. (2000) Oxidation of atmospheric methane in Nothern European soils, comparison with other ecosystems, and uncertainties in the global terristrial sink, *Global Change Biol. 6*, 791−803.
3. Smith, T. J., and Dalton, H. (2004) Biocatalysis by methane monooxygenase and its application to the petroleum industry, in *Petroleum Biotechnology, Developments and Perspectives* (Vazquez-Duhalt, R., and Quentero-Ramirez, R., Eds.) pp 177−192, Elsevier Science, BV, Amsterdam, The Netherlands.
4. DiSpirito, A. A., Gulledge, J., Shiemke, A. K., Murrell, J. C., Lidstrom, M. E., and Krema, C. L. (1992) Trichloroethylene oxidation by the membrane associated methane monooxygenase in type I, II and X methanotrophs, *Biodegradation 2*, 151−164.
5. Hanson, R. S., and Hanson, T. E. (1996) Methanotrophic bacteria, *Microbiol. Rev. 60*, 439−471.
6. Prior, S. D., and Dalton, H. (1985) The effect of copper ions on membrane content and methane monooxygenase activity in methanol-grown cells *Methylococcus capsulatus* (Bath), *J. Gen. Microbiol. 131*, 155−163.
7. Murrell, J. C., Gilbert, B., and McDonald, I. R. (2000) Molecular biology and regulation of methane monooxygenase, *Arch. Microbiol. 173*, 325−332.
8. Stanley, S. H., Prior, S. D., Leak, D. J., and Dalton, H. (1983) Copper stress underlies the fundamental change in intracellular location of methane monooxygenase in the methane-oxidizing organizms: studies in batch and continuous cultures, *Biotechnol. Lett. 5*, 487−492.
9. Green, J., and Dalton, H. (1985) Protein B of soluble methane monooxygenase from *Methylococus capsulatus* (Bath), *J. Biol. Chem. 260*, 15795−15801.
10. Ward, N., Larsen, Q., Sakwa, J., and Bruseth, L. (2004) Genomic insights into methanotrophy: The complete genome sequence of *Methylococcus capsulatus* (Bath), *PLoS Biol. 2*(10), e303.
11. Murrell, J. C. (1994) Molecular genetics of methane oxidation, *Biodegradation 5*, 145−159.

12. Rosenzweig, A. C., Frederick, C. A., Lippard, S. J., and Nordlund, P. (1993) Crystal-structure of a bacterial nonheme iron hydroxylase that catalyzes the biological oxidation of methane, *Nature (London) 366*, 537−543.
13. Lieberman, R. L., and Rosenzweig, A. C. (2005) Crystal structure of membrane-bound metalloenzyme that catalyses the biological oxidation of methane, *Nature (London) 434*, 177−182.
14. Colby, J., Stirling, D. I., and Dalton, H. (1977) The soluble methane monooxygenase of *Methylococcus capsulatus* (Bath): its ability to oxygenate n-akanes, n-alkenes, ethers, and acyclic, aromatic and heterocyclic compounds, *Biochem. J. 165*, 395−402.
15. Nguyen, H. H. T., Elliott, S. J., Yip, J. H.-K., and Chan, S. I. (1998) The particulate methane monooxygenase from *Methylococcus capsulatus* (Bath) is a novel copper-containing three-subunit enzyme, *J. Biol. Chem. 273*, 7957−7966.
16. Zahn, J. A., and DiSpirito, A. A. (1996) Membrane-associated methane monooxygenase from *Methylococcus capsulatus* (Bath), *J. Bacteriol. 178*, 1018−1029.
17. DeWitt, J. G., Bentsen, J. G., Rosenzweig, A. C., Hedman, B., Green, J., Pilkington, S., Papaefthymiou, G. C., Dalton, H., Hodgson, K. O., and Lippard, S. J. (1991) X-ray absorption, Mossbauer and EPR studies of the dinuclear iron center in the hydroxylase component of methane monooxygenase, *J. Am. Chem. Soc. 113*, 9219−9235.
18. Shiemke, A. K., Cook, S. A., Miley, T., and Singleton, P. (1995) Detergent solubilization of membrane-bound methane monooxygenase requires plastoquinol analogs as electron donors, *Arch. Biochem. Biophys. 321*, 421−428.
19. Lund, J., and Dalton, H. (1985) Further characterization of the FAD and Fe_2S_2 redox centers of component C, the NADH:acceptor reductase of the soluble methane monooxygenase of *Methylococcus capsulatus* (Bath), *Eur. J. Biochem. 147*, 291−296.
20. Anthony, C., and Williams, P. G. (2003) The structure and mechanism of methanol dehydrogenase, *Biochim. Biophys. Acta 1647*, 18−23.
21. Brantner, C. A., Remsen, C. C., Owen, H. A., Buchholz, L. A., and Collins, M. L. P. (2002) Intracellular localization of the particulate methane monooxygenase and methanol dehydrogenase in *Methylomicrobium album BGS*, *Arch. Microbiol. 178*, 59−64.
22. Ghosh, R., and Quayle, J. R. (1981) Purification and properties of the methanol dehydrogenase from *Methylophilus methylotrophus*, *Biochem. J. 199*, *245−250*.
23. Wadzinski, A. M., and Ribbons, D. W. (1975) Oxidation of C_1 compounds by particulate fractions from *Methylococcus capsulatus*: properties of methanol oxidase and methanol dehydrogenase, *J. Bacteriol. 122*, 1364−1374.
24. Whittenbury, R., Phillips, K. C., and Wilkinson, J. F. (1970) Enrichment, isolation and some properties of methane utilising bacteria, *J. Gen. Microbiol. 61*, 205−218.
25. Kitmitto, A., Myronova, N., Basu, P., and Dalton, H. (2005) Characterization and structural analysis of an active particulate methane monooxygenase trimer from *Methylococcus capsulatus (*Bath), *Biochemistry 44*, 10954−10965.
26. Lowry, O. H., Rosebrough, N. G., Farr, A. L., and Randall, R. J. (1951) Protein measurement with the Folin phenol reagent, *J. Biol. Chem. 193*, 265−275.
27. Day, D., and Anthony, C. (1990) Methanol dehydrogenase from *Methylobacterium extorquens* AM1, *Methods Enzymol. 188*, 210−216.
28. Schagger, H. (2003) Blue native electrophoresis, in *Membrane protein purification and crystallization* (Hunte, C., Von Jagov, G., and Schagger, H., Eds.) pp 105−130, Academic Press, London and New York.
29. Schagger, H., and Von Jagov, G. (1991) Blue native electropheresis for isolation of membrane protein complexes in enzymatically active form, *Anal. Biochem. 199*, 223−231.
30. Laemmli, U. K. (1970) Cleavage of the structural proteins during the assembly of the head of the bacteriophage T4, *Nature (London) 227*, 680−685.
31. Schuck, P. (2000) Size-distribution analysis of macromolecules by sedimentation velocity ultracentrifugation and Lamm equation modelling, *Biophys. J. 78*, 1606−1619.
32. Lebowitz, J., Levis, M. S., and Schuck, P. (2002) Modern analytical ultracentrifugation in protein science, *Protein Sci. 11*, 2067−2079.
33. Hoppert, M., and Holzenburg, A. (1998) Preparation techniques for transmission electron microscopy (TEM), in *Electron Microscopy in Microbiology: RMS Handbook Series* (Hoppert, M., and Holzenburg, A., Eds.) pp 11−18, BIOS Scientific Publishers Ltd., Oxford.
34. Ludtke, S. J., Baldwin, P. R., and Chiu, W. (1999) EMAN: Semiautomated software for high-resolution single-particle reconstructions, *J. Struct. Biol. 128*, 82−97.
35. Bottcher, B., Wynne, S. A., and Crowther, R. A. (1997) Determination of the fold of the core protein of hepatitis B virus by electron microscopy, *Nature (London) 386*, 88−91.
36. Harauz, G., and Vanheel, M. (1986) Exact filtres for general geometry 3-Dimensional reconstruction, *Optik 73*, 146−156.
37. Smith, D. D. S., and Dalton, H. (1989) Solubilisation of methane monooxygenase from *Methylococcus capsulatus* (Bath), *Eur. J. Biochem. 182*, 667−671.
38. Boumans, H., Grivell, L. A., and Berden, J. (1998) The respiratory chain in yeast behaves as a single functional unit, *J. Biol. Chem. 273*, 4872−4877.
39. Schagger, H., and Pfeiffer, K. (2000) Supercomplexes in the respiratory chains of yeast and mammalian mitochondria, *EMBO J. 19*, 1777−1783.
40. Stroh, A., Anderka, O., Pfeiffer, K., Yagi, T., Finel, M., Ludwig, B., and Schagger, H. (2004) Assembly of respiratory complex I, III, and IV into NADH oxidase supercomplex stabilizes complex I in *Paracoccus denitrificans*, *J. Biol. Chem. 279*, 5000−5007.
41. Boekema, E. J., van Breemen, J. F. L., van Roon, H., and Dekker, J. P. (2000) Conformation changes in photosystem II supercomplexes upon removal of extrinsic subunits, *Biochemistry 39*, 12907−12915.
42. Blake, C., Ghosh, M., Harlos, K., Avezoux, A., and Anthony, C. (1994) The active site of methanol dhydrogenase contains a disulfide bridge between adjacent cysteine residues, *Nat. Struct. Biol. 1*, 102−105.
43. Xia, Z. X., He, Y. N., Dai, W. W., White, S. A., Boyd, G. D., and Mathews, F. S. (1999) Detailed active site configuration of a new crystal form of methanol dehydrogenase from *Methylophilus methylotrophus* W3A1 at 1.9 angstrom resolution, *Biochemistry 38*, 1214−1220.
44. Hartmann, W. K., Saptharishi, N., Yang, X. Y., Mitra, G., and Soman, G. (2004) Characterization and analysis of thermal denaturation of antibodies by size exclusion high-performance liquid chromatoghraphy with quadruple detection, *Anal. Biochem. 325*, 227−239.
45. Suarez, M. D., Revzin, A., Narlock, R., Kempner, E. S., Thompson, D. A., and Fergusonmiller, S. (1984) The functional and physical form of mammalian cytochrome-c oxidase determinated by gel-filtration, radiation inactivation, and sedimentation equilibrium analysis, *J. Biol. Chem. 259*, 3791−3799.
46. Choi, D.-W., Kunz, R. C., Boyd, E. C., Semrau, J. D., Antholine, W. E., Han, J.-I., Zahn, J. A., Boyd, J. M., de la More, A. M., and DiSpirito, A. A. (2003) The membrane-associated methane monooxygenase (pMMO) and pMMO−NADH:quinone oxidoreductase complex from *Methylococcus capsulatus* Bath, *J. Bacteriol. 185*, 5755−5764.
47. Lieberman, R. L., and Rosenzweig, A. C. (2005) The quest for particulate methane monooxygenase active site, *Dalton Trans.*, 3390−3395.
48. Miled, N., Bussetta, C., De caro, A., Riviere, M., Berti, L., and Canaan, S. (2003) Importance of lid and cap domains for the catalytic activity of gastric lipases, *Comp. Biochem. Physiol., Part B 136*, 131−138.
49. Leak, D. J., and Dalton, H. (1986 a) Growth yields of methanotrophs 1. Effect of copper on the energetics of methane oxidation, *Appl. Microbial. Biotechnol. 23*, 470−476.
50. Anthony, C. (1978) The production of growth yields in methanotrophs, *J. Gen. Microbiol. 104*, 91−104.
51. Tonge, G. M., Harrison, D. E. F., Knowles, C. J., and Higgins, I., J. (1975) Properties and partial purification of the methane-oxidizing enzyme system from *Methylosinus trichosporium*, *FEBS Lett. 58*, 293−299.
52. Leak, D. J., and Dalton, H. (1986 b) Growth yields of methanotrophs 2. A theoretical analysis, *Appl. Microbiol. Biotechnol. 23*, 477−481.

BI061294P